Seismogenic width controls aspect ratios of earthquake ruptures

Huihui Weng[1] [iD] **and Hongfeng Yang[1]** [iD]

[1]Earth System Science Programme, Faculty of Science, Chinese University of Hong Kong, Sha Tin, Hong Kong

Abstract We investigate the effect of seismogenic width on aspect ratios of earthquake ruptures by using numerical simulations of strike-slip faulting and an energy balance criterion near rupture tips. If the seismogenic width is smaller than a critical value, then ruptures cannot break the entire fault, regardless of the size of the nucleation zone. The seismic moments of these self-arresting ruptures increase with the nucleation size, forming nucleation-related events. The aspect ratios increase with the seismogenic width but are smaller than 8. In contrast, ruptures become breakaway and tend to have high aspect ratios (>8) if the seismogenic width is sufficiently large. But the critical nucleation size is larger than the theoretical estimate for an unbounded fault. The eventual seismic moments of breakaway ruptures do not depend on the nucleation size. Our results suggest that estimating final earthquake magnitude from the nucleation phase may only be plausible on faults with small seismogenic width.

1. Introduction

Estimating potential rupture extent and seismic moment has significant implication for assessing seismic risk. Scaling relationships between seismic moment and along-strike length and down-dip width of rupture extents for large earthquakes have been extensively compiled [e.g., *Romanowicz*, 1992; *Scholz*, 1994; *Leonard*, 2010]. The debate on this scaling has focused on whether the coseismic slip and stress drop are determined by the width (i.e., *W* model) [*Romanowicz and Ruff*, 2002] or by the length (i.e., *L* model) [*Scholz*, 1994] of the rupture. Based on new data sets and numerical simulations, it has been accepted that the seismogenic width may determine the coseismic slip and stress drop [*Day*, 1982a; *Manighetti et al.*, 2007]. It has also been suggested that the down-dip width of seismogenic zones may limit the maximum earthquake magnitude [*Hyndman*, 2007; *Ruff and Kanamori*, 1983]. For instance, the down-dip width of the Mariana subduction zone of ~40 km would limit the earthquake magnitude along the Mariana trench to 7.5 [*Hyndman*, 2007; *Yoshida et al.*, 1992]. However, the intrinsic physical limit of the seismogenic width on earthquake magnitude remains poorly understood.

Numerical simulations of rupture propagation are usually conducted to investigate rupture and nucleation processes [e.g., *Weng et al.*, 2016; *Yang et al.*, 2012]. Numerous reports have derived the critical size of nucleation zones to initiate breakaway ruptures. In these cases, ruptures propagate along the seismogenic faults continually if seismogenic zones are sufficiently large (termed as "unbounded" in this study) [*Ampuero et al.*, 2002; *Andrews*, 1976; *Bizzarri*, 2010; *Day*, 1982b; *Galis et al.*, 2015; *Uenishi and Rice*, 2003; *Weng et al.*, 2015; *Xu et al.*, 2015]. However, an expected breakaway rupture may become self-arresting on a seismogenically limited fault. This underscores the importance of detailed investigations of how a limited seismogenic zone may affect earthquake size [*Weng et al.*, 2016; *Madariaga and Olsen*, 2000]. Indeed, natural faults have finite seismogenic widths due to the temperature-induced brittle to ductile transition [*Ruff and Kanamori*, 1983]. The seismogenic widths of strike-slip faults are usually less than 20–30 km according to the finite fault rupture models of earthquakes (Figures 1a and 1b). Although earthquakes may occur in the upper mantle [*Zhu and Helmberger*, 1996; *Inbal et al.*, 2016], the seismogenic depth is still limited and usually smaller than the along-strike length of the faults (Figures 1a and 1b). Can earthquakes rupture the entire along-strike distance given the limited seismogenic width? In this study, we address this question by using 3-D dynamic rupture simulations that explore the effects of a seismogenically bounded fault on rupture nucleation, propagation, and termination. We find whether the nucleation process that can develop into a breakaway rupture is determined not only by the nucleation size but also by the seismogenic width, which holds important implication on assessing earthquake risk.
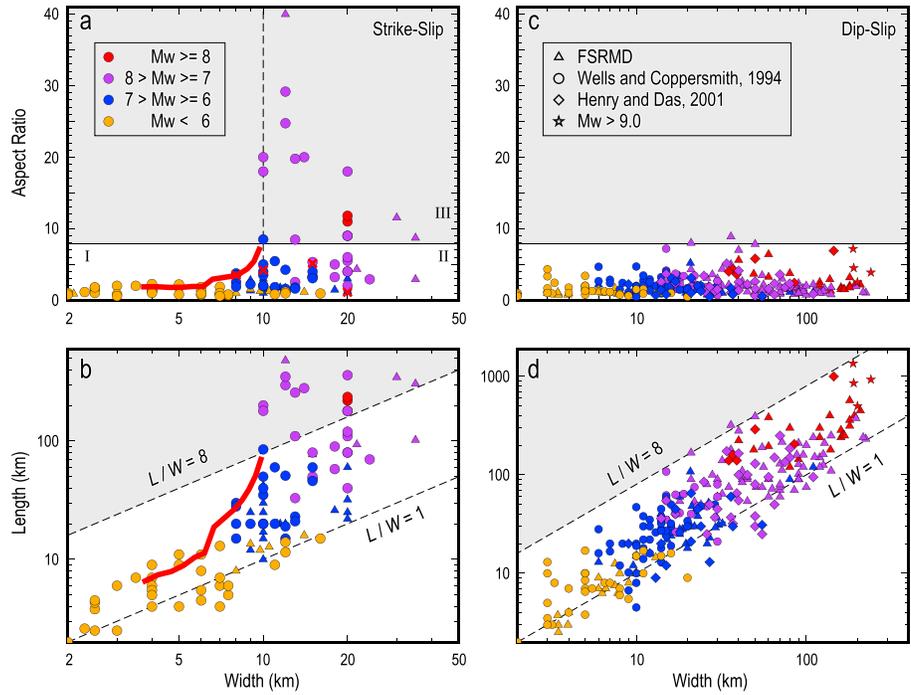
Figure 1. (a) Aspect ratio versus rupture width of strike-slip earthquakes. The gray region marks aspect ratio larger than 8. The red curve indicates the calculated aspect ratio from our simulated models without the free surface. The red crosses mark several strike-slip earthquakes in *Ellsworth and Beroza* [1995]. The dashed line marks the critical width. (b) Length versus width of rupture extent of strike-slip earthquakes. The dashed lines mark different aspect ratios. (c) Same as Figure 1a but for dip-slip earthquakes. (d) Same as Figure 1b but for dip-slip earthquakes. These catalogs are from *Wells and Coppersmith* [1994], *Henry and Das* [2001], and the online FSRMD database [*Mai and Thingbaijam*, 2014]. The stars mark the four $M_w > 9$ megathrust earthquakes.

2. Method

We consider a planar strike-slip fault embedded in a homogeneous elastic domain (Figure S1a in the supporting information). To simplify rupture models and gain insights into the physics of rupture propagation, we apply absorbing boundary condition on all boundaries and uniform material properties for all the simulated models: $V_P = 5.77$ km/s, $V_S = 3.33$ km/s, shear modulus $\mu = 30$ GPa, and Poisson's ratio $v = 0.25$. In a few cases, we set the upper boundary as a free surface and allow ruptures to propagate to the free surface (Figure S1b). Unless mentioned otherwise, all the following results refer to cases without the free surface.

The seismogenic fault locates in the center of the domain and is governed by a linear slip-weakening friction law [*Ida*, 1972], in which the friction coefficient f is given by

$$f(\delta) = \begin{cases} f_s - (f_s - f_d)\delta/d_0 & \delta \leq d_0 \\ f_d & \delta > d_0 \end{cases} \quad (1)$$

where f_s is the static friction coefficient, f_d is the dynamic friction coefficient, δ is the fault slip, and d_0 is the characteristic slip-weakening distance. Fault slips are constrained inside the seismogenic fault. We choose a uniform ambient effective normal stress for simplicity (i.e., $\sigma_n = 50$ MPa). All the fault parameters outside the nucleation zone are uniform

Table 1. Fault Parameters

Fault Parameter	Value
Static friction coefficient, f_s	0.63
Dynamic friction coefficient, f_d	0.54
Effective normal stress, σ_n (MPa)	50
$\tau_s - \tau_d$, (MPa)	4.5
Initial shear stress, τ_0 (MPa)	29
$\tau_0 - \tau_d$, (MPa)	2
Initial shear stress (nucleation), τ_0^i (MPa)	31.51
Critical slip distance, d_0 (m)	0.2

(Table 1). To initiate ruptures we set the shear stress inside the nucleation zone slightly higher than the static strength (Table 1). For most models in this study, the nucleation patches are set up as circles.

The critical nucleation size for breakaway ruptures on an unbounded fault can be estimated by using the following equation [*Galis et al.*, 2015]:

$$R_{\text{nuc}} = \frac{\pi}{4} \frac{1}{f_{\text{min}}^2} \frac{\tau_s - \tau_d}{(\tau_0 - \tau_d)^2} \mu d_0 \qquad (2)$$

where R_{nuc} is the critical nucleation radius and τ_0, τ_s, and τ_d are the initial shear stress and static and dynamic shear stresses, respectively. $\tau_s = \sigma_n f_s$ and $\tau_d = \sigma_n f_d$. f_{min} is the minimum of the function

$$f(x) = \sqrt{x} \left[1 + \frac{\tau_0^i - \tau_0}{\tau_0 - \tau_d} \left(1 - \sqrt{1 - 1/x^2} \right) \right] \qquad (3)$$

where τ_0^i is the initial shear stress inside the nucleation zone (Table 1). In this study the radii of nucleation zones R for all simulated models are larger than R_{nuc}, so that all nucleation patches should develop into breakaway ruptures if the faults are unbounded.

We set the seismogenic fault as a rectangle region and define the seismogenic width as W (Figure S1). We define the eventual length of rupture extents as L. To get more insights into rupture physics, we normalize W, L, and R to $W^* = W/\Lambda$, $L^* = L/\Lambda$, and $R^* = R/\Lambda$, respectively, where Λ is

$$\Lambda = \frac{\tau_s - \tau_d}{(\tau_0 - \tau_d)^2} \mu d_0 \qquad (4)$$

In addition, the final fault slip u is normalized to $u^* = u/[(\tau_0 - \tau_d)\Lambda/\mu]$ and the seismic moment M_0 is normalized to $M_0^* = M_0 / [(\tau_0 - \tau_d)\Lambda^3]$. Dynamic rupture simulations are conducted by using a finite element code, PyLith [*Aagaard et al.*, 2013]. The size of the cohesive zone in this study is ~1.6 km according to the following formula [*Day et al.*, 2005]:

$$\Pi_0 = \frac{9\pi}{32} \frac{\mu}{1 - \nu} \frac{d_0}{\tau_s - \tau_d} \qquad (5)$$

The grid size and time step are set to be 200 m and 0.01 s, respectively, that well satisfy numerical requirements (eight elements inside the cohesive zone).

3. Results

The seismogenic width plays a key role in the critical size of nucleation zones for breakaway ruptures (Figure 2). For the unbounded fault, if the nucleation size is larger than the critical value ($R_{\text{nuc}}^* = 0.30$), then the rupture will become breakaway. When bounding the seismogenic zone to a finite width, such as $W^* = 1.36$, the rupture can still break the entire seismogenic zone (Figure 2a), even if the fault length is doubled, indicating that it is also a breakaway rupture. The rupture speed and maximum slip rate on fault increase continuously as the rupture propagates (Figures S3a and S4a). However, the critical nucleation size (~0.36 for $W^* = 1.36$) for breakaway ruptures is larger than R_{nuc}^*. We conduct a series of simulations with various W^* and find that the critical size of nucleation zones increases as the seismogenic width decreases (as the arrow shows in Figure 3a).

In stark contrast, when the seismogenic width is reduced, e.g., $W^* = 1.13$, then the rupture will stop after propagating a short distance (Figure 2b), although the size of the nucleation zone is identical to the case of a breakaway rupture (Figure 2a). Even if we increase the nucleation size, e.g., a rectangle with an equivalent radius $R_{\text{equ}}^* = 0.71$, the rupture becomes self-arresting (Figure 2c). We use rectangular nucleation patches for those models whose equivalent radius R^* is larger than $W^*/2$. After experimenting with different seismogenic widths and nucleation sizes, we find that there exists a critical seismogenic width, smaller than which there are no breakaway ruptures no matter what the nucleation size is (Figure 3a). The critical width delineates a sharp boundary between the self-arresting and breakaway ruptures.

For the self-arresting ruptures, the eventual seismic moment depends on both the seismogenic width and the nucleation size (Figure 3a). In comparison, the seismic moment of breakaway ruptures is independent
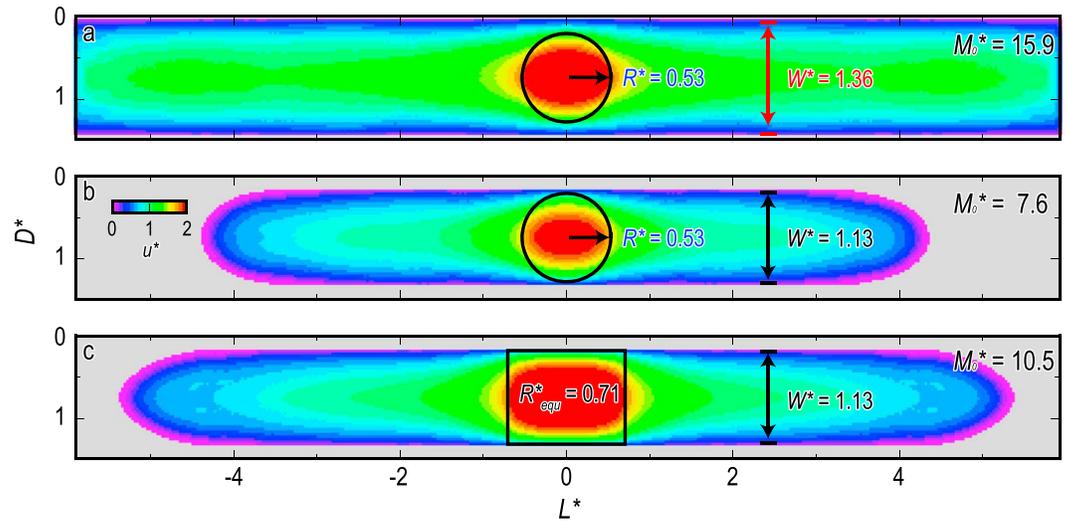
Figure 2. Coseismic slip distribution (color) for models with different seismogenic widths and nucleation sizes. (a) $R^* = 0.53$ and $W^* = 1.36$. (b) $R^* = 0.53$ and $W^* = 1.13$. (c) $R^*_{equ} = 0.71$ and $W^* = 1.13$. The black circles and rectangle mark the nucleation zones. L^* and D^* are normalized along-strike and down-dip distances. u^* is normalized coseismic slip. M_0^* is normalized seismic moment.

of the nucleation size. Given the same subcritical seismogenic width, the total eventual seismic moment increases rapidly with the nucleation size but tends to be "saturated" and even decreases for several seismogenic widths (Figure 3a). Because the higher shear stress inside the nucleation patches may contribute to the total seismic moment, we exclude the nucleation patches in calculating the seismic moment and find that the seismic moments have maxima for most subcritical seismogenic widths (Figure 3b). We extract the maximum seismic moments (without the contribution of the nucleation patches) for different seismogenic widths and find that the maximum seismic moment sharply increases with the seismogenic width (Figure 3c). In addition, the slope of the maximum seismic moment curve also increases with the seismogenic width and jumps to "infinite," i.e., breakaway ruptures, when the seismogenic width reaches the critical value (Figure 3c).

To investigate the intrinsic difference between the breakaway and self-arresting ruptures, we estimate the energy balance near rupture tips that plays a critical role in controlling the growth of ruptures. As a rupture
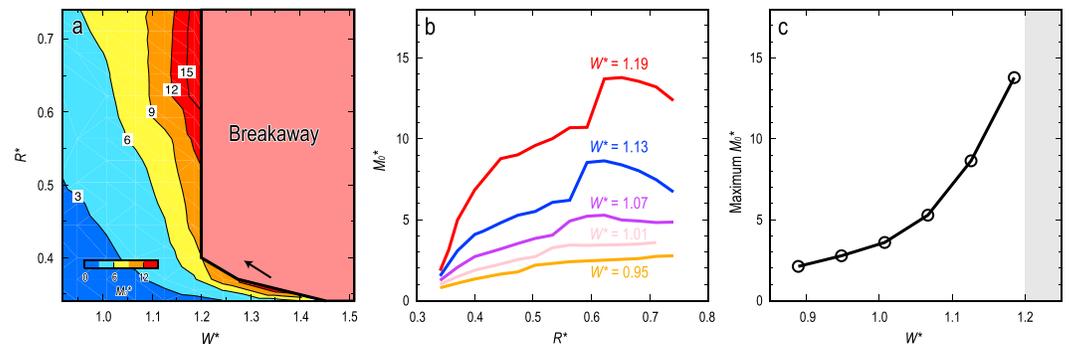
Figure 3. (a) Effects of seismogenic width W^* and nucleation size R^* on seismic moment. The thick black line separates two types of rupture: the breakaway and self-arresting ruptures. The black arrow shows that the critical nucleation size increases as the seismogenic width decreases. The contours in the self-arresting region mark the normalized seismic moment M_0^*. (b) Seismic moment versus size of nucleation zone for different seismogenic widths. Contribution from the nucleation patches has been deducted. (c) The maximum seismic moment as a function of seismogenic width. The gray rectangle marks the breakaway ruptures.
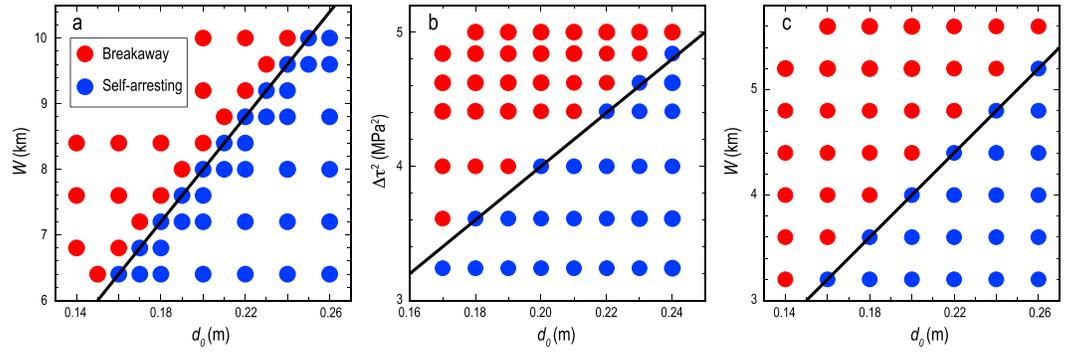
Figure 4. Effects of seismogenic width, critical slip-weakening distance and stress drop on rupture propagation. The red circles mark the breakaway ruptures, while the blue circles denote the self-arresting ruptures. The black lines mark the boundaries that satisfy the energy balance equation of $G = \mathcal{G}$ in the main text. (a) For models without the free surface: $\Delta\tau = 2$ MPa, $R = 3.2$ km. All other parameters are kept constant (Table 1). (b) For models without the free surface: W = 8 km, $R = 3.2$ k. (c) For models with the free surface: $\Delta\tau = 2$ MPa. The nucleation zone is a half circle ($R = 3.2$ km) with the diameter along the free surface.

propagates after saturating the seismogenic width, the rupture tip (cohesive zone) releases strain energy in an approximate rate [*Day*, 1982a]:

$$G \approx \frac{\pi}{2}\left(\frac{V_S}{V_R}\right)^2 \frac{\mathcal{R}(V_R)}{\sqrt{1 - \frac{V_R^2}{V_S^2}}} \cdot \frac{\Delta\tau^2}{\mu}W = A(V_R) \cdot \frac{\Delta\tau^2}{\mu}W \qquad (6)$$

where V_R is the rupture speed, A is a function of the rupture speed, $\Delta\tau = \tau_0 - \tau_d$, and $\mathcal{R}$ is the Rayleigh function

$$\mathcal{R}(c) = \left[\sqrt{1 - \frac{c^2}{V_P^2}}\sqrt{1 - \frac{c^2}{V_S^2}} - \left(1 - \frac{c^2}{2V_S^2}\right)^2\right] \qquad (7)$$

The value of A is shown in Figure S2 for the Poisson material. Meanwhile, the rupture tip needs to absorb energy to propagate further, which is termed fracture energy. For the linear slip-weakening friction law, the fracture energy is given by

$$\mathcal{G} = \frac{1}{2}(\tau_s - \tau_d)d_0 \qquad (8)$$

If the energy release rate is larger than the fracture energy (e.g., for larger W), then the rupture tip could accelerate as the rupture propagates (Figure S3a) and thus becomes breakaway. Otherwise the rupture cannot sustain and will become self-arresting. Therefore, the critical condition for breakaway ruptures shall be $G > \mathcal{G}$.

Next, we conduct a number of simulations for different W, $\Delta\tau$, and d_0 to test this critical condition, by fixing other parameters (Table 1). We find that the boundaries between the breakaway and self-arresting ruptures can be approximated by the energy balance equation of $G = \mathcal{G}$, i.e., $W/d_0 = \frac{\mu(\tau_s - \tau_d)}{2A\Delta\tau^2} \approx 40$ km/m for $\Delta\tau = 2$ MPa (Figure 4a) and $\Delta\tau^2/d_0 = \frac{\mu(\tau_s - \tau_d)}{2AW} \approx 20$ (MPa)^2/m for W = 8 km (Figure 4b), where $A \approx 0.43$ is estimated by using $V_R = 0.6V_S$. For the cases with a free surface, the approximate boundary is $W/d_0 \approx 20$ km/m (Figure 4c). Assuming $d_0 = 0.4$ m, the critical value of W in the cases with a free surface is ~8 km, while the critical value of W is ~16 km in the cases without free surface. The difference is because the free surface can amplify fault motion and emanate backward rerupture phase, increasing both the mean slip rate and the strain energy near rupture tips [*Xu et al.*, 2014].

4. Discussion

Whether the magnitude of earthquakes depends on the nucleation process is a key question in earthquake physics. Several observations of strike-slip and dip-slip earthquakes suggest that the eventual seismic

moment may increase with the size of the nucleation zone, magnitude of which ranges from 1.1 to 8.1 [*Dodge et al.*, 1996; *Ellsworth and Beroza*, 1995]. However, it has also been proposed that the earthquake sizes may not be nucleation-related, based on both seismic observations of different events [*Abercrombie and Mori*, 1994; *Mori and Kanamori*, 1996] and numerical simulations [*Lapusta and Rice*, 2003]. Here we find that the final earthquake magnitude is largely affected by the seismogenic width (Figure 3a). If the seismogenic zone is sufficiently wide, then the rupture may become breakaway and the magnitude is independent of the nucleation size. This has been concluded also from simulations in the framework of rate-state friction [*Lapusta and Rice*, 2003]. On the contrary, the initial nucleation size can control the eventual earthquake magnitude if the seismogenic width of faults is smaller than the critical value ($W^* < 1.2$, Figure 3a). Our findings shed light on the debate that is induced by different observations.

The widths of rupture extents on nearly vertical strike-slip faults are usually less than 20–30 km (Figures 1a and 1b). There appears to be a boundary near the width of 10 km where the highest aspect ratio (the ratio between the length and width of rupture extent) increases drastically from ~2 to >8 (Figures 1a and 1b). Ruptures of high aspect ratios (e.g., >8), which we suggest as breakaway ruptures (quadrant III in Figure 1a), could occur only when the rupture width is larger than 10 km, i.e., the breakaway region (quadrants II and III in Figure 1a). In our simulation results, for the subcritical seismogenic width (<10 km), all ruptures are self-arresting and only produce low aspect ratios (quadrant I in Figure 1a). Moreover, the aspect ratio of self-arresting ruptures increases with the seismogenic width (red curve in Figure 1a), which could serve as an upper limit of the observations. Breakaway ruptures in our models could propagate along the faults continually and produce sufficiently high aspect ratios when the width is larger than 10 km, well consistent with the observations.

Rupture propagation is also affected by a few other factors such as nonuniform stress distribution [*Yang et al.*, 2012], geometrical anomaly on the fault [*Yang et al.*, 2013], and heterogeneous fault zone materials [e.g., *Yang and Zhu*, 2010; *Yang et al.*, 2011, 2014; *Yang*, 2015; *Weng et al.*, 2016]. These factors can stop a breakaway rupture, resulting in a much lower rupture aspect ratio. In addition, the subcritical nucleation may cause self-arresting ruptures for all seismogenic widths (Figure 3a), including unbounded faults [*Xu et al.*, 2015]. All these conditions may be the reasons for the observed events with low aspect ratios that are located within our defined breakaway region (quadrant II in Figure 1a), including several nucleation-related earthquakes suggested in *Ellsworth and Beroza* [1995] (red crosses in Figure 1a).

Contrast to strike-slip events, nearly all dip-slip earthquakes in Figure 1c have aspect ratios smaller than 8. Moreover, their rupture lengths scale linearly with the rupture widths, mostly bounded by the lines of aspect ratios of 1 and 8 (Figure 1d). An intriguing feature is that there appears to be no sudden change of aspect ratio. The difference in aspect ratios of strike-slip and dip-slip earthquakes may stem from the variance in stress drop or fracture energy. According to equation (6), there is a trade-off between the seismogenic width and the stress drop in estimating the energy release rate near rupture tips, i.e., $G \propto \Delta\tau^2 W$. Although the seismogenic widths of dip-slip faults could be ~5–15 times larger than those of strike-slip faults, the average stress drop of strike-slip earthquakes may be 3–5 times (9–25 times for $\Delta\tau^2$) larger than that of dip-slip events [*Allmann and Shearer*, 2009]. Therefore, the average energy release rate of dip-slip earthquakes is probably smaller than that of strike-slip earthquakes, which may lead to the absence of high aspect ratios of dip-slip earthquakes. Alternatively, if the energy release rate of dip-slip earthquakes is comparable to that of strike-slip events, then we expect that the average fracture energy of dip-slip faults should be systematically larger than that of strike-slip faults, which is worth of further investigation.

5. Conclusions

The seismogenic width plays an important role in rupture propagation on vertical strike-slip faults. The approximate energy release rate near rupture tips for bounded faults is linearly proportional to the seismogenic width. If the seismogenic width is smaller than the critical width, then the rupture will become self-arresting and the eventual seismic moment and aspect ratio increase with both the seismogenic width and the nucleation size. These findings provide a plausible mechanism to those earthquakes observed to have nucleation-related seismic moments. If the seismogenic width is larger than the critical width, then the rupture can become breakaway and tends to have a high aspect ratio. The seismic moment is independent of the nucleation size. The results suggest that estimating eventual earthquake magnitude from

observing the nucleation phase may only be plausible on faults with small seismogenic widths, providing important implications for assessing seismic risk.

References

Aagaard, B., M. Knepley, and C. Williams (2013), A domain decomposition approach to implementing fault slip in finite-element models of quasi-static and dynamic crustal deformation, *J. Geophys. Res. Solid Earth*, 118, 3059–3079, doi:10.1002/jgrb.50217.

Abercrombie, R., and J. Mori (1994), Local observations of the onset of a large earthquake: 28 June 1992 Landers, California, *Bull. Seismol. Soc. Am.*, 84(3), 725–734.

Allmann, B. P., and P. M. Shearer (2009), Global variations of stress drop for moderate to large earthquakes, *J. Geophys. Res.*, 114, B01310, doi:10.1029/2008JB005821.

Ampuero, J. P., J. P. Vilotte, and F. Sanchez-Sesma (2002), Nucleation of rupture under slip dependent friction law: Simple models of fault zone, *J. Geophys. Res.*, 107(B12), 2324, doi:10.1029/2001JB000452.

Andrews, D. J. (1976), Rupture propagation with finite stress in antiplane strain, *J. Geophys. Res.*, 81(20), 3575–3582, doi:10.1029/JB081i020p03575.

Bizzarri, A. (2010), How to promote earthquake ruptures: Different nucleation strategies in a dynamic model with slip-weakening friction, *Bull. Seismol. Soc. Am.*, 100(3), 923–940.

Day, S. (1982a), Three-dimensional finite difference simulation of fault dynamics: Rectangular faults with fixed rupture velocity, *Bull. Seismol. Soc. Am.*, 72(3), 705–727.

Day, S. (1982b), Three-dimensional simulation of spontaneous rupture: The effect of nonuniform prestress, *Bull. Seismol. Soc. Am.*, 72(6A), 1881–1902.

Day, S. M., L. A. Dalguer, N. Lapusta, and Y. Liu (2005), Comparison of finite difference and boundary integral solutions to three-dimensional spontaneous rupture, *J. Geophys. Res.*, 110, B12307, doi:10.1029/2005JB003813.

Dodge, D. A., G. C. Beroza, and W. Ellsworth (1996), Detailed observations of California foreshock sequences: Implications for the earthquake initiation process, *J. Geophys. Res.*, 101(B10), 22,371–22,392, doi:10.1029/96JB02269.

Ellsworth, W., and G. Beroza (1995), Seismic evidence for an earthquake nucleation phase, *Science*, 268(5212), 851.

Galis, M., C. Pelties, J. Kristek, P. Moczo, J.-P. Ampuero, and P. M. Mai (2015), On the initiation of sustained slip-weakening ruptures by localized stresses, *Geophys. J. Int.*, 200(2), 890–909, doi:10.1093/gji/ggu436.

Henry, C., and S. Das (2001), Aftershock zones of large shallow earthquakes: Fault dimensions, aftershock area expansion and scaling relations, *Geophys. J. Int.*, 147(2), 272–293.

Hyndman, R. (2007), The seismogenic zone of subduction thrust faults, in *The Seismogenic Zone of Subduction Thrust Faults*, edited by T. H. Dixon and J. C. Moore, pp. 15–40, Columbia Univ. Press, New York.

Ida, Y. (1972), Cohesive force across the tip of a longitudinal-shear crack and Griffith's specific surface energy, *J. Geophys. Res.*, 77(20), 3796–3805, doi:10.1029/JB077i020p03796.

Inbal, A., J. P. Ampuero, and R. W. Clayton (2016), Localized seismic deformation in the upper mantle revealed by dense seismic arrays, *Science*, 354(6308), 88–92.

Lapusta, N., and J. R. Rice (2003), Nucleation and early seismic propagation of small and large events in a crustal earthquake model, *J. Geophys. Res.*, 108(B4), 2205, doi:10.1029/2001JB000793.

Leonard, M. (2010), Earthquake fault scaling: Self-consistent relating of rupture length, width, average displacement, and moment release, *Bull. Seismol. Soc. Am.*, 100(5A), 1971–1988, doi:10.1785/0120090189.

Madariaga, R., and K. B. Olsen (2000), Criticality of rupture dynamics in 3-D, *Pure Appl. Geophys.*, 157(11–12), 1981–2001.

Mai, P. M., and K. Thingbaijam (2014), SRCMOD: An online database of finite-fault rupture models, *Seismol. Res. Lett.*, 85(6), 1348–1357.

Manighetti, I., M. Campillo, S. Bouley, and F. Cotton (2007), Earthquake scaling, fault segmentation, and structural maturity, *Earth Planet. Sci. Lett.*, 253(3), 429–438.

Mori, J., and H. Kanamori (1996), Initial rupture of earthquakes in the 1995 Ridgecrest, California sequence, *Geophys. Res. Lett.*, 23(18), 2437–2440, doi:10.1029/96GL02491.

Romanowicz, B. (1992), Strike-slip earthquakes on quasi-vertical transcurrent faults: Inferences for general scaling relations, *Geophys. Res. Lett.*, 19(5), 481–484, doi:10.1029/92GL00265.

Romanowicz, B., and L. Ruff (2002), On moment-length scaling of large strike slip earthquakes and the strength of faults, *Geophys. Res. Lett.*, 29(12), 1604, doi:10.1029/2001GL014479.

Ruff, L., and H. Kanamori (1983), Seismic coupling and uncoupling at subduction zones, *Tectonophysics*, 99(2), 99–117.

Scholz, C. (1994), A reappraisal of large earthquake scaling, *Bull. Seismol. Soc. Am.*, 84(1), 215–218.

Uenishi, K., and J. R. Rice (2003), Universal nucleation length for slip-weakening rupture instability under nonuniform fault loading, *J. Geophys. Res.*, 108(B1), 2042, doi:10.1029/2001JB001681.

Wells, D. L., and K. J. Coppersmith (1994), New empirical relationships among magnitude, rupture length, rupture width, rupture area, and surface displacement, *Bull. Seismol. Soc. Am.*, 84(4), 974–1002.

Weng, H., J. Huang, and H. Yang (2015), Barrier-induced supershear ruptures on a slip-weakening fault, *Geophys. Res. Lett.*, 42, 4824–4832, doi:10.1002/2015GL064281.

Weng, H., H. Yang, Z. Zhang, and X. Chen (2016), Earthquake rupture extents and coseismic slips promoted by damaged fault zones, *J. Geophys. Res. Solid Earth*, 121, 4446–4457, doi:10.1002/2015JB012713.

Xu, J., H. Zhang, and X. Chen (2015), Rupture phase diagrams for a planar fault in 3-D full-space and half-space, *Geophys. J. Int.*, 202(3), 2194–2206.

Xu, S., E. Fukuyama, F. Yamashita, K. Mizoguchi, S. Takizawa, and H. Kawakata (2014), Evolution of rupture style with accumulation of fault displacement during large-scale biaxial friction experiments, Abstract T13E-05 presented at 2014 Fall Meeting, AGU, San Francisco, Calif.

Yang, H. (2015), Recent advances in imaging crustal fault zones: A review, *Earthquake Sci.*, 28(2), 151–162, doi:10.1007/s11589-015-0114-3.

Yang, H., and L. Zhu (2010), Shallow low-velocity zone of the San Jacinto fault from local earthquake waveform modelling, *Geophys. J. Int.*, 183(1), 421–432, doi:10.1111/j.1365246X.2010.04744.x.

Yang, H., L. Zhu, and E. S. Cochran (2011), Seismic structures of the Calico fault zone inferred from local earthquake travel time modelling, *Geophys. J. Int.*, 186(2), 760–770, doi:10.1111/j.1365-246X.2011.05055.x.

Yang, H., Y. Liu, and J. Lin (2012), Effects of subducted seamounts on megathrust earthquake nucleation and rupture propagation, *Geophys. Res. Lett.*, 39, L24302, doi:10.1029/2012GL053892.

Yang, H., Y. Liu, and J. Lin (2013), Geometrical effects of a subducted seamount on stopping megathrust ruptures, *Geophys. Res. Lett.*, *40*, 2011–2016, doi:10.1002/grl.50509.

Yang, H., Z. Li, Z. Peng, Y. Ben-Zion, and F. Vernon (2014), Low-velocity zones along the San Jacinto Fault, Southern California, from body waves recorded in dense linear arrays, *J. Geophys. Res. Solid Earth*, *119*, 8976–8990, doi:10.1002/2014JB011548.

Yoshida, Y., K. Satake, and K. Abe (1992), The large normal-faulting Mariana earthquake of April 5, 1990 in uncoupled subduction zone, *Geophys. Res. Lett.*, *19*(3), 297–300, doi:10.1029/92GL00165.

Zhu, L., and D. V. Helmberger (1996), Intermediate depth earthquakes beneath the India-Tibet Collision Zone, *Geophys. Res. Lett.*, *23*(5), 435–438, doi:10.1029/96GL00385.